The Inhibition of ATP-Dependent Shape Change of Human Erythrocyte Ghosts Correlates With an Inhibition of Mg^{2+}-ATPase Activity by Fluoride and Aluminofluoride Complexes

Michael B. Morris, Gregory Monteith, and Basil D. Roufogalis

Department of Pharmacy, University of Sydney, Sydney 2006, Australia

Abstract   The vanadate-sensitive Mg^{2+}-dependent ATPase activity of the human erythrocyte ghost is believed to be involved in the shape change events that convert echinocytic ghosts to smoothed forms (biconcave discs and stomatocytes). At physiological salt concentration, pH 7.4, 2 mM ATP, 5 mM Mg^{2+} and 1 mM EGTA, the Mg^{2+}-ATPase activity of ghosts was inhibited strongly by millimolar concentrations of sodium fluoride: I_{50} = 1.31 ± 0.23 mM (mean ± S.D.; n = 12). The addition of aluminium chloride to 15 μM reduced the concentration of NaF required for 50% inhibition to 0.76 ± 0.21 mM (n = 10). Aluminium alone had only a small inhibitory effect on the ATPase activity (13 ± 9%; n = 10). Desferrioxamine, a strong chelator of tervalent aluminium ion, failed to reverse the inhibition by fluoride and reversed the inhibition in the presence of aluminium and fluoride back to those values obtained with fluoride alone. Of several metal salts tested only beryllium sulfate was able to replace aluminium as an effective inhibitor in the presence of fluoride.

Inhibition of the Mg^{2+}-ATPase activity by fluoride and the aluminofluoride complexes correlated with an inhibition of the rate of MgATP-dependent change in red cell ghost shape from echinocytes to smoothed forms. All gross morphological changes of the smoothing process were affected, including the production of discocytes, stomatocytes and endocyctic vesicles.

Key words: echinocyte, discocyte, stomatocyte, endocytosis, phosphate analogue, desferrioxamine, beryllium

A Mg^{2+}-dependent ATPase activity in the human red cell membrane appears to be responsible for maintaining the resting biconcave shape of intact red blood cells and for controlling the smoothing of intact red cells and echinocytic red cell ghosts to biconcave discs and stomatocytes [1–5].

The mechanism of this shape change remains unclear nor has a definite function been ascribed to the purported Mg^{2+}-ATPase(s). The direct involvement of a protein kinase which phosphorylates one or more of the major cytoskeletal proteins or band 3 (the anion transporter) seems unlikely [1,4], although a small amount of phosphorylation of a major structural protein, or the rapid and extensive phosphorylation of a minor

protein, cannot be excluded as possible mechanisms [2,3]. Furthermore, phosphorylation of various membrane structural proteins is known to affect the strength of protein-protein interactions critical to the shape, stability and deformability of the red cell [6–9]. These results suggest that protein phosphorylation may play a role in shape change which is secondary to the mechanism involving the Mg^{2+}-ATPase activity.

Vanadate partially inhibits the Mg^{2+}-ATPase activity in erythrocyte ghosts and this inhibition correlates with an inhibition of the transformation of echinocytic ghosts to smoothed forms [10]. Vanadate also accelerates the rate of echinocytosis in intact, discocytic red cells during ATP depletion [4,11]. Vanadate inhibition suggests that a P-type (phosphoprotein intermediate) transport Mg^{2+}-ATPase may be involved. If so, however, there is no net pumping of H^{+}, SO$_4^{2-}$, Mg^{2+}, or Rb^{+} by this enzyme activity [12]. Backman [4] has shown that the acceleration of echinocytosis by vanadate in intact, discocytic

red cells partially correlates with an increase in the rate of dephosphorylation of phosphatidyl-inositolbisphosphate on the inner leaflet of the lipid bilayer, thereby implying the involvement of a lipid kinase/phosphatase. The reduction in area of the inner leaflet due to lipid dephosphorylation has been calculated to be sufficient to promote echinocytosis [13]. Alternatively, the lipid translocase of the erythrocyte membrane also depends on MgATP hydrolysis and is vanadate sensitive [14] and the loss of lipid asymmetry may result in echinocytosis. In both cases, inhibition of ATP hydrolysis presumably results from vanadate acting as a transition-state analogue of phosphate in the active site of these enzymes [15].

In contrast, aluminofluoride and beryllofluoride complexes act as ground-state phosphate analogues [16–18]. These metallofluoride complexes inhibit a number of different types of phosphotransfer reaction, including ATP hydrolysis by ion-pump enzymes with a P-type mechanism, such as sarcoplasmic reticulum $(Ca^{2+} + Mg^{2+})$-ATPase and Na^+/K^+-ATPase [19]; F-type ATPases [20]; enzymes, such as glucose-6-phosphatase, involved in the phosphorylation state of metabolites [21]; GTP hydrolysis by G-proteins [22,23] and the hydrolysis of ATP by actin and GTP by tubulin under polymerizing conditions [24,18]. In the case of hydrolysis of ATP or GTP, the metallofluoride complexes are predicted to mimic the terminal phosphate of the nucleotide and thereby inhibit enzyme turnover by a number of related mechanisms [15].

Fluoride alone also inhibits phosphotransfer reactions, such as those catalysed by asymmetrical Ap_4A hydrolases [25] and phosphatases [26–29], as well as inhibiting the activity of other enzymes, such as enolase [30].

In this paper we examine the inhibition of the Mg^{2+}-ATPase activity of the red cell ghost by fluoride, aluminofluoride complexes, and beryllofluoride complexes. Inhibition of the Mg^{2+}-ATPase activity by fluoride and the aluminofluoride complexes correlates with an inhibition of the ability of echinocytic ghosts to undergo smoothing to discocytes and stomatocytes.

MATERIALS AND METHODS
Materials

Na_2EDTA, Na_2EGTA, ouabain, Malachite Green, Tween 20, and PMSF were obtained from Sigma. Na_2ATP was obtained from Sigma

(cat. no. A5394) or Boehringer Mannheim (cat. no. 519 979). $AlCl_3$ was highest-quality grade obtained from Merck. NaF was obtained from the following sources: Laboratory grade NaF was obtained from Ajax Chemicals (Sydney, Australia) and May and Baker (Dagenham, England); analytical grade was obtained from BDH and Ajax Chemicals. Desferrioxamine methylsulfonate (Desferal) was obtained from Ciba-Geigy. Glutaraldehyde was from Bio-Rad.

Preparation of Erythrocyte Ghosts

Ghosts were prepared as described [31] with the following modifications: 1–10 mL freshly-collected, packed red cells were washed twice with 2–4 volumes of buffer containing 10 mM Tris (pH 7.5 at 25°C)/150 mM NaCl/0.4 mM phenylmethylsulfonyl fluoride (PMSF) and the cells centrifuged for 1 min at 12,000g in 50 mL tubes. Washed cells were lysed and the haemoglobin removed by 2–3 washes with 10 mM Tris (pH 8 at 25°C)/1 mM EDTA/0.04 mM PMSF. The ratio of lysing buffer to packed red cells ranged from 100–300:1 between preparations. After each wash, ghosts were collected by centrifugation for 10 min at 16,000g in 250 mL tubes. EDTA and PMSF were removed by two washes with ~100 volumes of 10 mM Tris, pH 7.4 and collecting the white ghosts by centrifugation. Ghosts were stored in a polycarbonate vial at 4°C.

Concentration of protein in the ghosts was determined spectrophotometrically after dissolving the ghosts in 2% SDS. The concentration was determined from the absorbance at 280 nm (corrected for light scattering at 350 nm) using an extinction coefficient of $E_{1cm}^{1\%} = 14.4$. The value for the extinction coefficient was obtained by relating the corrected absorbance at 280 nm with the concentration of protein obtained from a Bradford microprotein assay (Bio-Rad) using bovine serum albumin as a standard. S.E. Lux and K. John (Children's Hospital, Boston), using the protein assay of Lowry, have determined an $E_{1cm}^{1\%} = 14.4$ at 280 nm for ghosts dissolved in 1% SDS.

Determination of Mg^{2+}-ATPase Activity

Mg^{2+}-ATPase activity in ghosts was determined by quantitating the release of free phosphate from ATP using the method of Lanzetta et al. [32] adapted to a microplate reader. In a typical experiment 9 volumes of ghosts (0.75

g/L) in 10 mM Tris were added to 1 volume of 10× Buffer A (31 mM Tris, pH 7.4 at 25°C/1.4 M KCl/50 mM MgCl$_2$/10 mM EGTA/1 mM ouabain). To 4 volumes of these ghosts were added 1 volume of Buffer A (12 mM Tris, pH 7.4 at 25°C/140 mM KCl/5 mM MgCl$_2$/1 mM EGTA/0.1 mM ouabain) containing 1) 83.3 μM AlCl$_3$ or 2) NaF (0–55.6 mM) or 3) AlCl$_3$ in combination with NaF. (The use of glassware and concentrated stocks of NaOH and HCl was avoided because of potential contamination by aluminium [23]. However, we obtained similar results in all experiments even if these precautions were not taken.)

Duplicate 54 μL aliquots of the samples were transferred to individual wells in a 96-well Titertek microplate (Flow Laboratories). The plate was placed in a shaking water bath at 37°C. ATP hydrolysis in each column of wells was initiated by the introduction of 6 μL of ATP solution (20 mM Na$_2$ATP/1 mM ouabain in Buffer A containing 43 mM Tris, pH 7.4 at 25°C) using a multichannel pipette.

Reactions were stopped after a fixed time between 50 and 70 min with 160 μL/well of Malachite Green solution [32], followed immediately by adequate mixing with 30 μL/well 34% sodium citrate.2H$_2$O (w/v). For controls, duplicate 54 μL aliquots were incubated at 37°C without ATP then ATP, colour solution and citrate were added in rapid succession. After 30–90 min colour development at room temperature, the 96-well plate was transferred to a Bio-Rad 3550 microplate reader and the absorbances recorded at 655 nm. The average standard deviation for duplicates was ~2%. The colour complex was stable for at least 20 h.

The same assay procedure was used to test the effect of ZnSO$_4$, MnSO$_4$, CuSO$_4$, and BaCl$_2$ (each at a final assay concentration of 15 μM) and BeSO$_4$ (50–500 nM final assay concentration) on Mg^{2+}-ATPase activity.

Desferrioxamine (0.5 or 2 mM final assay concentration) was added to ghosts after being dissolved in Buffer A containing NaF ± AlCl$_3$, as required. In some experiments, desferrioxamine in Buffer A was added to ghosts suspended in Buffer A and the mixture incubated overnight at 4°C before the addition of NaF and/or AlCl$_3$. The final assay concentration of desferrioxamine was 2 mM.

Each microplate contained phosphate standards (0–10 nmol/60 μL) made from a stock of anhydrous K$_2$HPO$_4$. After colour development, 10 nmol phosphate gave a blank-corrected absorbance of 2.0–2.3 depending on the assay. The response was linear over the absorbance range with correlation coefficients of ≥ 0.997 and ordinate intercepts very close to the origin.

Shape Change Assay

The shape change assay was performed essentially as described by Patel and Fairbanks [1]. Immediately upon preparation of white ghosts, the ghosts were diluted to 0.075 g/L protein with ice-cold 10 mM Tris (pH 7.4 at 25°C). These swollen, smooth ghosts were made echinocytic by the addition of 0.11 volumes of ice-cold 10× Buffer A. Echinocytic ghosts then were divided into 1.01 mL aliquots to which were added 252 μL of ice-cold stocks of NaF (0–55.6 mM) ± 83.3 μM AlCl$_3$ in Buffer A.

Shape change was initiated by the addition of 140 μL aliquots of ATP solution, followed immediately by plunging of the tubes into a 30°C shaking water bath. At known time intervals, aliquots were removed from the ghost suspensions and fixed with an equal volume of ice-cold fixing solution (10 mM sodium phosphate, pH 7.4/140 mM KCl/2% glutaraldehyde). ATP-independent smoothing was monitored in identical fashion but excluding ATP.

The shapes of fixed ghosts were assessed using phase contrast on a Zeiss III RS light microscope fitted with a Ph3 Neofluar 100× oil immersion lens with the Optovar at 1.25×. Ghosts were classified as echinocytic, discocytic, or stomatocytic according to the usual rules applied to intact erythrocytes [33], but with the following ammendments: Because of the difficulty in distinguishing early stage echinocytes (echinocytes I) from the smooth contours of the discocyte, echinocytes I were classified as discocytes. In some cases, discocyte-shaped ghosts were covered with up to ~50 small black dots, presumably representing the final vestiges of echinocytic spicules withdrawing into the body of the membrane. These ghosts were classified as discocytes unless projecting spicules also could be observed. Some discocyte-like ghosts observed edge on possessed highly angular contours, although no spicules could be observed. These ghosts were classified as echinocytes since separate observations showed that such cells, while rotating before settling, were distinctly spiculated. Ghosts containing endocytic vesicles were counted separately as a subset of stomatocytes.
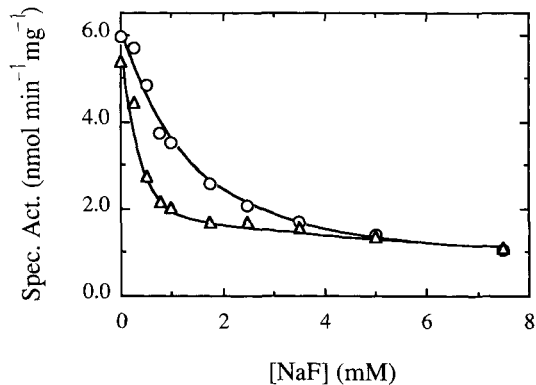
Fig. 1. Inhibition of the Mg^{2+}-ATPase activity of erythrocyte ghosts by increasing concentrations of NaF (O) and by fluoride in the presence of 15 μM $AlCl_3$ (△).
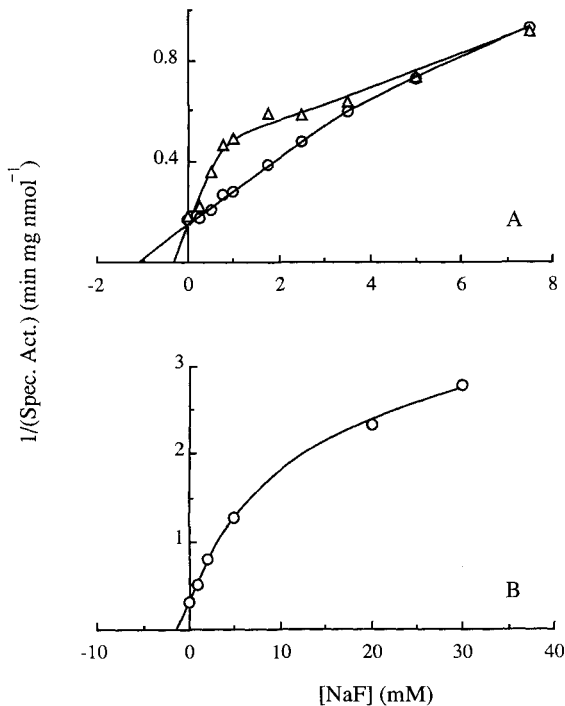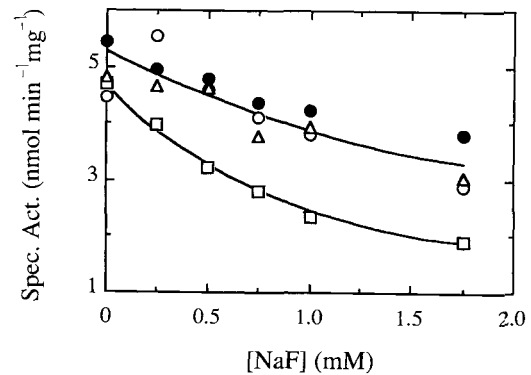

Fig. 3. The effect of desferrioxamine on the inhibition of the Mg^{2+}-ATPase activity of erythrocyte ghosts by NaF and fluoride plus $AlCl_3$. Final concentrations of added compounds were as follows: (O) control ghosts (no additions); (●) 0.5 mM desferrioxamine; (□) 15 μM $AlCl_3$; (△) 15 μM $AlCl_3$ plus 0.5 mM desferrioxamine.

Fig. 2. Dixon plots of data obtained from the inhibition of Mg^{2+}-ATPase activity in erythrocyte ghosts by NaF alone (O) or by fluoride in the presence of 15 μM $AlCl_3$ (△). **Panel A** represents the transformation of data in Figure 1. **Panel B** presents a different set of data showing curvature of the Dixon plot at higher concentrations of fluoride in the absence of aluminium.

RESULTS

Inhibition of Mg^{2+}-ATPase Activity by Fluoride and Aluminium

Figure 1 shows the result of a typical experiment in which the Mg^{2+}-ATPase activity in white

ghosts was inhibited by NaF in a dose-dependent manner. The results from 12 experiments showed that 1.31 ± 0.23 mM fluoride (mean ± S.D.) was required to inhibit Mg^{2+}-ATPase activity by 50%. At concentrations of fluoride above ~3 mM, Mg^{2+}-ATPase activity declined slowly. More than 10% of the Mg^{2+}-ATPase activity remained in the presence of 30 mM fluoride (Fig. 2B).

Fifteen μM $AlCl_3$ added to ghosts resulted in only a small inhibitory effect on activity (13 ± 9%; n = 10). However, the combination of fluoride and aluminium shifted the inhibition curve to the left (Fig. 1), with 0.76 ± 0.21 mM fluoride (n = 10) required to inhibit 50% of the activity remaining after the addition of aluminium alone. The size of the shift was dependent upon the concentration of aluminium: 30 μM aluminium shifted the inhibition curve even further to the left (data not shown).

Seventy to eighty percent of the Mg^{2+}-ATPase activity was highly sensitive to inhibition by the combination of fluoride and aluminium. However, as with fluoride alone, the final 20–30% of activity was largely insensitive to inhibition. Inhibition by fluoride and fluoride plus aluminium was reversible by > 80%, either by dialysis against 100 volumes of Buffer A for several hours at 4°C or by pelleting the ghosts, removing the supernatant, and resuspending the ghosts in Buffer A, free of inhibitors.

Figure 2A shows that Dixon plots of data obtained in the presence of fluoride alone tended to curve downward, especially at higher concentrations of fluoride (Fig. 2B). In some experi-
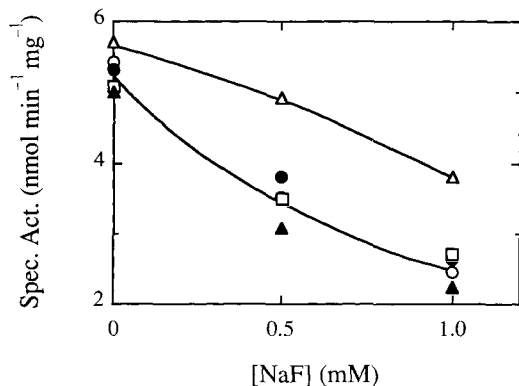
Fig. 4. Inhibition of the Mg^{2+}-ATPase activity of erythrocyte ghosts by four different metal salts in the presence of increasing concentrations of NaF. Final concentrations of metal salts were as follows: (O) control ghosts (no additions); (●) 15 μM $CuSO_4$; (△) 15 μM $BaCl_2$; (▲) 15 μM $MnSO_4$; (□) 15 μM $ZnSO_4$. The calculated [40,41] concentrations of metal ion not complexed with ATP and EGTA in the absence of fluoride were as follows: Cu^{2+}, < 1 pM; Ba^{2+}, 472 nM; Mn^{2+}, 64 pM; Zn^{2+}, 24 pM. The concentration of aluminium not complexed with ATP and EGTA under these conditions was < 1 pM.
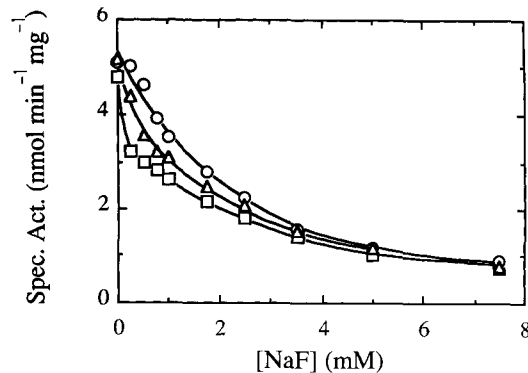

Fig. 5. Inhibition of the Mg^{2+}-ATPase activity of the erythrocyte ghost by $BeSO_4$ in the presence of increasing concentrations of fluoride. Final concentrations of $BeSO_4$ (nM) were as follows: (O) 0; (△) 50; (□) 500. Specific activity was determined by the release of inorganic phosphate following incubation for 60 min at 37°C (see Materials and Methods for details).

ments, Dixon plots in the presence of fluoride alone were distinctly biphasic (data not shown). Dixon plots of data obtained in the presence of aluminium were always distinctly biphasic (Fig. 2A).

Tests With Desferrioxamine

Many commercial preparations of ATP contain aluminium as their major metal contaminant [34]. In order to reduce the possibility that the effect of added fluoride was due simply to complexing with contaminating aluminium, we added 0.5 mM desferrioxamine to some assay samples. Desferrioxamine is an extremely strong chelator of Al^{3+} ($K_a = 10^{22}$ M^{-1}) [35]. Figure 3 shows that desferrioxamine did not alter the inhibition of the Mg^{2+}-ATPase by fluoride in the absence of added aluminium. In the presence of 15 μM added aluminium, the inhibition curve is again shifted to left, but with aluminium in the presence of desferrioxamine the curve is shifted back to that obtained with fluoride alone. Similar results were obtained with 2 mM desferrioxamine.

Overnight incubation of ghosts with desferrioxamine failed to reverse the inhibition observed with fluoride alone. This indicates that fluoride was not reacting with contaminating aluminium in the ghosts and forming an occluded complex which inhibited Mg^{2+}-ATPase activity.

Other contaminants within NaF stocks, which are not chelated by desferrioxamine, may be responsible for the inhibition observed in the presence of fluoride alone. However, this seems unlikely since four different sources of NaF were used (ranging from laboratory grade to analytical grade) and each gave identical results.

Inhibition of Mg^{2+}-ATPase Activity by Other Metal Ions

Figure 4 shows three other metal ions (Cu^{2+}, Mn^{2+}, Zn^{2+}) failed to inhibit Mg^{2+}-ATPase activity in the presence and absence of fluoride. Ba^{2+} consistently activated the Mg^{2+}-ATPase activity to a small extent in the presence of fluoride (Fig. 4). This may result from stimulation of the (Ca^{2+} + Mg^{2+})-ATPase [36]. $BeSO_4$, on the other hand, strongly inhibited the Mg^{2+}-ATPase activity in the presence of fluoride. Figure 5 shows that inhibition curves with various fixed concentrations of $BeSO_4$ and increasing concentrations of fluoride are similar to those obtained for aluminium (Fig. 1). However, $BeSO_4$ proved to be effective at submicromolar concentrations.

Inhibition of ATP-Dependent Ghost Smoothing

The ability of erythrocyte ghosts to change shape from the echinocytic forms to the smoothed forms (discocytes and stomatocytes) in the presence of fluoride and fluoride plus aluminium also was examined. As expected, ghosts in 10 mM Tris appeared smooth and expanded under the phase contrast microscope [1]. Upon the addition of salt to physiological

**TABLE I. Inhibition of the
Mg^{2+}-ATPase Activity After the Addition of
Various Combinations of NaF and $AlCl_3$***

Additions	% Full activity
None ($\bigcirc$)	100[a]
15 μM $AlCl_3$ ($\bullet$)	105
1 mM NaF ($\triangle$)	69
0.3 mM NaF + 15 μM $AlCl_3$ ($\blacktriangle$)	75
1.75 mM NaF ($\square$)	48
1 mM NaF + 15 μM $AlCl_3$ ($\blacksquare$)	41
3.5 mM NaF ($\diamondsuit$)	29
3.5 mM NaF + 15 μM $AlCl_3$ (+)	25

*This preparation of ghosts and the additions used here were employed in the shape change assay displayed in Figures 6 and 7. The symbols in brackets represent those used in Figures 6 and 7.

[a]The specific activity of control ghosts was 5.8 nmol min^{-1} mg^{-1}.

concentration, the ghosts became echinocytic. The degree of echinocytosis varied between ghost preparations. In some ghost preparations, the addition of salt gave rise largely to echinocytes II, with some echinocytes III and, in some cases, a small percentage (< 10%) of discocytes. In most preparations, the ghosts were more heavily spiculated and no smoothed forms were present. These differences between experiments may be due to the speed with which ghosts were prepared and used in the shape change experiments [1]. However, irrespective of the degree of echinocytosis after the addition of salt, the trends in smoothing of the ghosts, after addition of ATP and incubation at 30°C, were the same.

Figure 6 shows that the rate of production of smoothed forms was progressively inhibited by increasing concentrations of fluoride in both the presence and absence of 15 μM aluminium. The degree of inhibition appears to correlate with the Mg^{2+}-ATPase activity (Table I). Thus, for example, 1 mM fluoride substantially inhibited smoothing ($\triangle$, Fig. 6) but 1 mM fluoride in the presence of aluminium ($\blacksquare$) was more effective, consistent with the greater inhibition of the Mg^{2+}ATPase activity (Table I).

Note that in the presence of 15 μM aluminium alone ($\bullet$, Fig. 6), smoothing was slightly inhibited, even though the Mg^{2+}-ATPase activity was not affected (Table I). In this experiment, this difference is most apparent at 5 min, where the percentage of smoothed forms in the

presence of aluminium was less than two-thirds that for control ghosts ($\bigcirc$). In all other experiments this difference was more marked and sustained over longer time periods. Similarly, smoothing was more strongly inhibited by combinations of fluoride and aluminium that inhibited Mg^{2+}-ATPase activity to a degree similar to that obtained with fluoride alone. Thus, for example, the combination of 0.3 mM fluoride plus 15 μM aluminium ($\blacktriangle$, Fig. 6) inhibited smoothing more strongly than 1 mM fluoride alone ($\triangle$, Fig. 6), even though Mg^{2+}-ATPase activity was inhibited by ~ 30% in both cases (Table I).

ATP-dependent production of smoothed forms was completely eliminated when the Mg^{2+}-ATPase activity was inhibited by 70–80%, whether this was achieved by fluoride alone or by the combination of fluoride plus aluminium. This generally occurred with 3.5 mM fluoride present, although in some experiments (as in Fig. 6), a small amount of ATP-dependent smoothing was still apparent under these conditions.

Some ATP-independent smoothing also was observed in the experiment in Figure 6 (~ 18%) [see 1,10]. However, in no case was this affected by fluoride and/or aluminium compared with control ghosts. ATP-independent smoothing varied from 0–30% depending on the ghost preparation, but did not proceed beyond the discocyte stage in any experiment.

The effect of inhibitors on the production of the various shapes of ghosts during the smoothing process also was examined. Figure 7A shows that the MgATP-dependent production of discocytes in control ghosts reached a maximum of ~ 50% after 5 min and thereafter declined rapidly to zero. The reason for this maximum formation and subsequent decline is that the discocytes were progressively transformed to stomatocytes. In the presence of 1 mM fluoride, the initial rate of production of discocytes was slower than for control ghosts, the maximum production was delayed from 5 min to 15 min and the subsequent decline was slower, indicating a slower conversion to stomatocytes in the presence of inhibitor. Thus, in general, the initial rate of production of discocytes, as well as their rate of decline, was reduced progressively as the Mg^{2+}-ATPase activity was inhibited (Fig. 7A,B; Table I).

Similarly, the production of stomatocytes (Fig. 7C) and endocytic vesicles (Fig. 7D) appears to correlate with the inhibition of the Mg^{2+}-
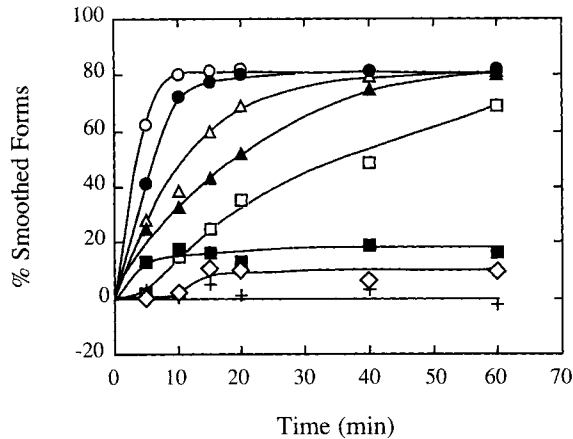
Fig. 6. The effect of NaF and the combination of fluoride plus AlCl₃ on the ATP-dependent smoothing of echinocytic erythrocyte ghosts at 30°C. Ghosts in ice-cold 10 mM Tris were made echinocytic by the addition of a concentrated stock of ice-cold KCl followed by the addition of ice-cold stocks of NaF or NaF plus AlCl₃. Smoothing was initiated by the addition of a stock solution of ATP followed by plunging of the sample tubes into a 30°C water bath. Aliquots were withdrawn at specified times, fixed with glutaraldehyde, and the shapes of the ghosts were examined under phase contrast (for details see Materials and Methods). Final concentrations of fluoride and aluminium were as follows: (○) no additions; (●) 15 μM AlCl₃; (△) 1 mM NaF; (▲) 0.3 mM NaF plus 15 μM AlCl₃; (□) 1.75 mM NaF; (■) 1 mM NaF plus 15 μM AlCl₃; (◇) 3.5 mM NaF; (+) 3.5 mM NaF plus 15 μM AlCl₃. Since there was no apparent dependence of ATP-independent shape change with NaF or AlCl₃ concentration, these data were grouped and smoothed by eye for each time point over the 60-min incubation period. These smoothed values were subtracted from those values obtained in the presence of ATP. ATP-independent smoothing reached a maximum of 18% and did not proceed beyond the discocyte stage.

ATPase activity (Table I). Note that in control ghosts the onset of production of endocytic vesicles lagged 5–10 min behind the onset of production of stomatocytes as a whole, and this lag time increased in the presence of fluoride and fluoride plus aluminium.

Another general feature of these experiments was that smoothing slowed markedly and sometimes ceased entirely during the incubation at 30°C. For example, Figure 8 shows the results from an experiment in which the smoothing of ghosts in 2.5 mM fluoride ceased after 20 min of incubation. The results from several experiments indicate that this phenomenon occurred independently of the presence of fluoride alone, aluminium alone, or fluoride plus aluminium, but rather was strongly time dependent and usually could be observed readily after 20 to 40 min of incubation. In control ghosts, this could be observed at the level of production of stomatocytes or endocytic vesicles (Fig. 8).

DISCUSSION

Fluoride and Metallofluoride Complexes Inhibit Mg²⁺-ATPase Activity

Increasing concentrations of fluoride in the millimolar range progressively inhibit the Mg²⁺-ATPase activity of the human erythrocyte ghost (Figs. 1, 3). The use of desferrioxamine showed that this inhibition was not due to the presence of contaminating aluminium (Fig. 3). The results of Antonny et al. [37], based on the activation of transducin, suggested to them that fluoride acts to entrap Mg²⁺ as MgF₃⁻ at that part of the active site where the γ-phosphate of the nucleotide is normally held. A similar mechanism, with almost identical affinities for the entrapment of Mg²⁺, may operate for the Mg²⁺-ATPase activity of the ghost. If the mechanism is general, however, it must eventually account for the fact that fluoride is capable of inhibiting asymmetrical Ap₄A hydrolases at concentrations two orders of magnitude lower than those used here [25].

Aluminium (Fig. 1) and beryllium (Fig. 5) enhanced the inhibition by fluoride of the Mg²⁺-ATPase activity, presumably through the formation of metallofluoride complexes acting as ground-state phosphate analogues [15–17,38]. In general, it has proved difficult to ascertain the active metallofluoride species since, for both aluminium and beryllium, many species co-exist in solution and are non-covalent [17,18]. The ghost system is complicated by the fact that free fluoride is simultaneously inhibiting Mg²⁺-ATPase activity. In addition, Mg²⁺, ATP and EGTA will perturb the distributions of aluminofluoride species that are predicted to occur in aqueous solution [17] and lipids such as phosphatidylserine will bind certain aluminium species [39]. Indeed, of the total aluminium added (15 μM), most is complexed with EGTA and ATP and the calculated [40,41] free concentration is only picomolar. Thus, a maximum of 15 μM aluminium is available to complex with added fluoride, but only by redistribution of aluminium complexed with ATP and EGTA or bound to the membrane.

The inhibition curves using beryllofluoride complexes (Fig. 5) are very similar to those obtained using aluminofluoride (Fig. 1), but the concentration of beryllium needed to produce a similar level of inhibition is 30–100 times less than for aluminium. This may reflect the different degrees of chelation of Be²⁺ with EGTA
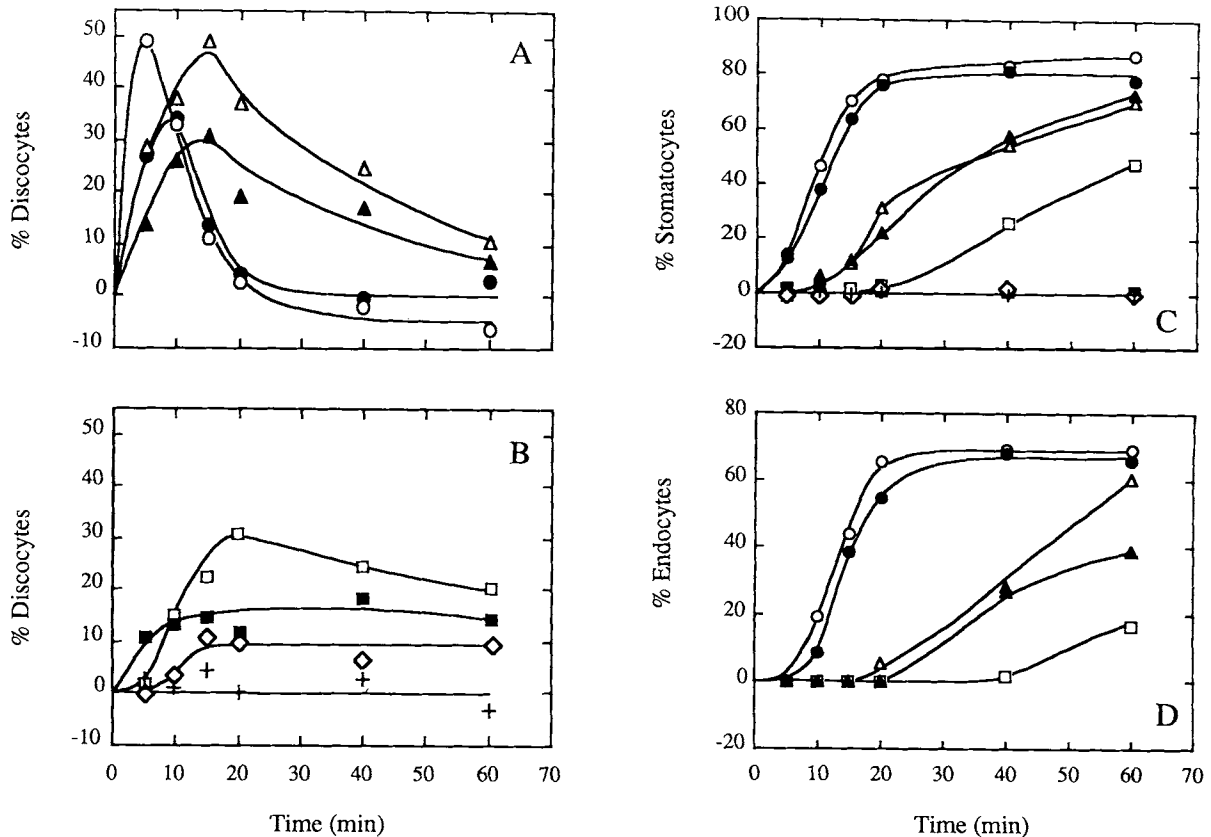
Fig. 7. The effect of NaF and the combination of fluoride plus AlCl₃ on the ATP-dependent production of discocytes, stomatocytes, and endocytic vesicles. Data are from the same experiment as Figure 6 (see legend to Fig. 6 and Materials and Methods for experimental details). **Panels A** and **B** show the production of discocytes only. These data have been split for clarity and have been plotted to the same scale. **Panel C** shows the production of stomatocytes only. **Panel D** shows the production of the subset of stomatocytes containing endocytic vesicles. No endocytic vesicles were produced with 1 mM NaF plus AlCl₃ or 3.5 mM NaF ± AlCl₃ and these data points have been omitted for clarity.

and ATP and/or different association constants for the formation of beryllofluoride complexes compared with aluminofluoride complexes [17]. In addition, beryllium, like aluminium, is capable of interacting with biological membranes [42].

Correlation Between Shape Change and Mg²⁺-ATPase Activity

There is a strong correlation between inhibition of the Mg²⁺-ATPase activity by fluoride and aluminofluoride complexes and inhibition of the smoothing process in ghosts (Figs. 6, 7; Table I). Similar correlations have been observed in studies with vanadate [10], N-substituted maleimides [43], Cd²⁺ and p-chloromercuribenzoate [44]. Furthermore, it is apparent that fluoride and aluminofluoride complexes affect the production of the full gamut of smoothed forms, including the production of endocytic vesicles. There are

at least three possible explanations for this observation: 1) A single mechanism is responsible for the production of all smoothed forms. 2) Two or more mechanisms are involved, each possibly responsible for the production of particular shapes and each with similar sensitivity to fluoride or aluminofluoride complexes. 3) Fluoride and aluminofluoride complexes only inhibit a rate-limiting mechanism responsible for the production of discocytes from echinocytes, thereby indirectly retarding the rate of production of stomatocytes and endocytic vesicles. Investigations are currently underway to distinguish among these possibilities.

Aluminium alone inhibited shape change quite significantly, even though its effect on the Mg²⁺-ATPase activity was very small (see, for example, Fig. 6, Table I). Similarly, combinations of fluoride and aluminium inhibited shape change
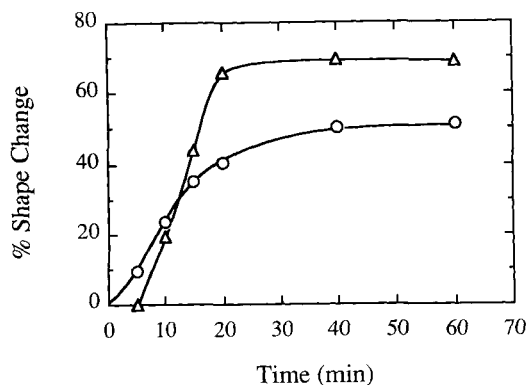
Fig. 8. Time-dependent cessation of smoothing of echinocytic erythrocyte ghosts (see legend to Fig. 6 and Materials and Methods for experimental details). (O) Percentage production of smoothed forms (discocytes and stomatocytes) for a preparation of echinocytic ghosts incubated with 2.5 mM NaF. (△) Percentage production of stomatocytes containing endocytic vesicles for a preparation of control ghosts. The two sets of data are from experiments performed on different preparations of ghosts and exemplify the observation that smoothing ceases or slows dramatically after 20–40 min of incubation at 30°C, independent of the concentration of added compounds such as NaF and/or AlCl₃. ATP-independent smoothing has not been subtracted from the data so that the theoretical maximum production of smoothed forms (O) and stomatocytes with endocytic vesicles (△) is 100%.

more markedly than fluoride alone, even if the Mg^{2+}-ATPase activity was inhibited to a similar extent (Fig. 6, Table I). Interactions between aluminium and other membrane components such as lipids [39] may serve to disable the ghosts by some means, making them less sensitive to ATP-dependent shape change.

Dissociation of Shape Change From Mg^{2+}-ATPase Activity

We and Patel and Fairbanks [1] have noted that ghosts kept at 4°C must be used within 1–2 h of preparation, after which time they lose their ability to change shape from echinocytes to smoothed forms. Presumably, this process is accelerated at 30°C (Fig. 8). Patel and Fairbanks [10] suggest that the cessation of shape change is due not only to the inherent lability of the process, but also to the depletion of ATP within partially resealed ghosts. However, the depletion of ATP in our ghosts seems unlikely, since ATP should be small enough to enter the ghost pore(s) [45]. In addition, ATP hydrolysis at 37°C remained linear for over 2 h (data not shown), indicating that saturating concentrations of ATP

were available to drive the shape change process.

In spite of the rapid loss of ability of ghosts to change shape, full Mg^{2+}-ATPase activity in stored ghosts persisted for many days after their preparation (data not shown). This could mean that the Mg^{2+}-ATPase activity is not involved in the smoothing of ghosts, but several other possibilities exist: 1) Only a small percentage of Mg^{2+}-ATPase activity may be associated with shape change and this activity may decline rapidly. In this case, the small percentage of activity responsible for the smoothing process, and the bulk of Mg^{2+}-ATPase activity, would need to have similar sensitivities to reagents such as fluoride and aluminofluoride complexes. Missiaen et al. [46] have observed a Mg^{2+}-ATPase activity in rat myometrium which is rapidly lost following the preparation of microsomes. 2) Alternatively, hydrolysis of ATP may persist but with the hydrolysis uncoupled from the function(s) of the Mg^{2+}-ATPase enzyme(s) involved. Our preliminary observations indicate that ghosts stored at 4°C in 10 mM Tris progressively lose the ability to undergo ATP-independent echinocytosis after the addition of salt, in addition to rapidly losing their ability to undergo MgATP-dependent smoothing. Thus, ghosts probably undergo many critical changes following (and probably during) their preparation; after 1–2 h at 4°C, the MgATP-dependent shape changing mechanism may still be intact and active, but smoothing is unable to proceed because of damage to other ghost components.

Mg^{2+}-ATPase Activity in Erythrocyte Ghosts May Consist of Two Components

Dixon plots of the inhibition of Mg^{2+}-ATPase activity by fluoride and aluminofluoride complexes (Fig. 2) are curved downwards, indicating that the inhibitors were not fully competitive with ATP assuming a single Mg^{2+}-ATPase enzyme, or that more than one type of Mg^{2+}-ATPase activity is present in the membrane.

Support for the possibility that two components are present comes from the observation that Dixon plots for inhibition by aluminofluoride are distinctly biphasic (Fig. 2A). Only 70–80% of the Mg^{2+}-ATPase activity is sensitive to inhibition by fluoride or aluminofluoride. This was sufficient to fully prevent echinocytic ghosts from smoothing to discocytes and stomatocytes and there did not appear to be any shift in the population of the various classes of echinocyte.

Therefore, the minor component of 20–30% activity does not appear to be involved in the shape change process (Figs. 6, 7; Table I).

Patel and Fairbanks [10] have shown that only 30% of the Mg^{2+}-ATPase activity is sensitive to vanadate ($I_{50} = 1$ μM) and that this level of inhibition is sufficient to completely inhibit smoothing. This again shows that there appears to be two components of Mg^{2+}-ATPase activity, but the relative percentage of the component involved with shape change differs markedly from our results. In contrast, we have found (Xu et al., unpublished results) that vanadate inhibition of the Mg^{2+}-ATPase activity is biphasic, with the major component representing 70–80% of the activity and having an I_{50} similar to that obtained by Patel and Fairbanks [10].

Possible Roles for the Mg^{2+}ATPase

The role of the Mg^{2+}-ATPase activity is currently postulated to be a phospholipid translocase based on its high specific activity, vanadate sensitivity, and possible inhibition by aluminofluoride complexes [47].

While it is certainly possible that fluoride and aluminofluoride complexes inhibit a single enzyme [37], the fact that fluoride is known to inhibit phosphatases [27] and phosphate analogues inhibit kinases [48] leaves open the possibility that a kinase/phosphatase cycle may be involved. Alternatively, some other multicomponent system may control MgATP-dependent smoothing with fluoride and aluminofluoride complexes affecting different components in the system.

The use of fluoride and metallofluoride complexes will help to determine if the phospholipid translocase or some other mechanism is associated with the Mg^{2+}-ATPase activity and ATP-dependent smoothing. In addition, these inhibitors have proved useful in our laboratory for monitoring the purification of Mg^{2+}-ATPase activities from the red cell membrane.

ACKNOWLEDGMENTS

REFERENCES

1. Patel VK, Fairbanks G: J Cell Biol 88:430, 1981.
2. Jinbu Y, Nakao M, Otsuka M, Sato S: Biochem Biophys Res Commun 112:384, 1983.
3. Jinbu Y, Sato S, Nakao M: Nature 307:376, 1984.
4. Backman L: J Cell Sci 80:281, 1986.
5. Schrier SL, Junga I, Ma L: Blood 68:1008, 1986.
6. Cianci CD, Giorgi M, Morrow JS: J Cell Biochem 37:301, 1988.
7. Lu P-W, Soong C-J, Tao M: J Biol Chem 260:14958, 1985.
8. Eder PS, Soong C-J, Tao M: Biochemistry 25:1764, 1986.
9. Danilov YN, Fennell R, Ling E, Cohen CM: J Biol Chem 265:2556, 1990.
10. Patel VK, Fairbanks G: J Biol Chem 261:3170, 1986.
11. Xu Y-H, Lu Z-Y, Conigrave AD, Auland ME, Roufogalis BD: J Cell Biochem 46:1, 1991.
12. Forgac M, Cantley L: J Memb Biol 80:185, 1984.
13. Ferrell JE, Heustis WH: J Cell Biol 98:1992, 1984.
14. Bitbol B, Fellmann P, Zachowski A, Devaux PF: Biochim Biophys Acta 904:268, 1987.
15. Chabre M: Trends Biochem Sci 15:6, 1990.
16. Bigay J, Deterre P, Pfister C, Chabre M: FEBS Lett 191:181, 1985.
17. Martin RB: Biochem Biophys Res Commun 155:1194, 1988.
18. Combeau C, Carlier MF: J Biol Chem 264:19017, 1989.
19. Missiaen L, Wuytack F, De Smedt H, Vrolix M, Casteels R: Biochem J 253:827, 1988.
20. Lunardi J, Dupuis A, Garin J, Issartel J-P, Michel L, Chabre M, Vignais PV: Proc Natl Acad Sci USA 85:8958, 1988.
21. Lange AJ, Arion WJ, Burchell A, Burchell B: J Biol Chem 261:101, 1986.
22. Kanaho Y, Moss J, Vaughan M: J Biol Chem 260:11493, 1985.
23. Sternweis PC, Gilman AG: Proc Natl Acad Sci USA 79:4888, 1982.
24. Carlier MF, Didry D, Melki R, Chabre M, Pantaloni D: Biochemistry 27:3555, 1988.
25. Guranowski A: FEBS Lett 262:205, 1990.
26. Bollen M, Stalmans W: Biochem J 255:327, 1988.
27. Brautigan DL, Shriner CL: Methods Enymol 159:339, 1988.
28. Ganzhorn AJ, Chanal M-C: Biochemistry 29:6065, 1990.
29. Kranias EG, Steenaart NAE, Di Salvo J: J Biol Chem 263:15681, 1988.
30. Berry MN, Gregory RB, Grivell AR, Henly DC, Phillips JW, Wallace PG, Welch GR: FEBS Lett 231:19, 1988.
31. Ralston GB, Dunbar JC: Biochim. Biophys. Acta 579:20, 1979.
32. Lanzetta PA, Alvarez LJ, Reinach PS, Candia OA: Anal Biochem 100:95, 1979.
33. Bessis M: In Bessis M, Weed RI, Leblond PF (eds): "Red Cell Shape: Physiology, Pathology, Ultrastructure." New York: Springer Verlag, 1973, pp 1–25.
34. Schloss JV, Smith G, Aulabaugh A, Cleland WW: Anal Biochem 120:176, 1982.
35. Blackmore PF, Bocckino SB, Waynick LE, Exton JH: J Biol Chem 260:14477, 1985.

36. Wins P, Schoffeniels E: Biochim Biophys Acta 120:341, 1966.
37. Antonny B, Bigay J, Chabre M: FEBS Lett 268:277, 1990.
38. Blackmore PF, Exton JH: J Biol Chem 261:11056, 1986.
39. Akeson MA, Munns DN, and Burau RG: Biochim Biophys Acta 986:33, 1989.
40. Goldstein DA: Biophys J 26:235, 1979.
41. Smith RM, Martell AE: In "Critical Stability Constants, Vol. 1 (1974), Vol. 2 (1975), Vol. 5 (1982)." New York: Plenum Press.
42. Stokinger HE: In Steere NV (ed): "CRC Handbook of Laboratory Safety, 2nd ed." Boca Raton, Florida: CRC Press, p 314.
43. Hayashi H, Penniston JT: Arch Biochem Biophys 159: 563, 1973.
44. Penniston JT: Arch Biochem Biophys 153:411, 1972.
45. Lieber MR, Steck TL: J Biol Chem 257:11651, 1982.
46. Missiaen L, Wuytack F, Casteels R: Biochem J 250:571, 1988.
47. Morrot G, Zachowski A, Devaux PF: FEBS Lett 266:29, 1990.
48. Macara IG: Trends Biochem Sci 5:92, 1980.